Optical Engineering 46(4), 048001 (April 2007)

Micrograting fabricated by deep x-ray lithography for optical communications

Cheng-Hao Ko
Yuan Ze University
Department of Electrical Engineering
135 Yuan Tung Rd.
Chungli 320, Taiwan
E-mail: ko.chenghao@gmail.com

Bor-Yuan Shew
National Synchrotron Radiation Research Center
101 Hsin-Ann Road
Hsinchu 300, Taiwan

Shih-Che Hsu
National Chiao-Tung University
Department of Mechanical Engineering
1001 Ta Hsueh Road
Hsinchu, Taiwan 300

Abstract. A concave micrograting designed for optical communication applications was fabricated by deep x-ray lithography (DXL). The micrograting has a height of 125 μm, a grating pitch of 3 μm, a total of 2584 lines, and a sidewall root-mean-square surface roughness of 5 nm. The designed operational wavelength range is from 1475 to 1625 nm. This micrograting is embedded inside a mirror-planar waveguide to form a spectrometer chip. The Rowland-circle grating mounting scheme is used for the spectral detection. The calculated diffraction efficiency of the third-order diffraction reaches 65% when Au is coated on the grating surface and the blaze angle is suitably chosen. The measured spectral width is 1.1 nm, which is in very good agreement with the calculated result of 0.9 nm. This chip-based grating device can be used as an ultracompact spectrometer or an ultracompact wavelength-division multiplexer in optical communications. Based on this work, our DXL technique can be further developed into an x-ray LIGA method for the mass production of such chip-based spectrometers. © 2007 Society of Photo-Optical Instrumentation Engineers. [DOI: 10.1117/1.2719709]

Subject terms: micrograting; x-ray lithography; DWDM; synchrotron radiation.

Paper 060305R received Apr. 24, 2006; revised manuscript received Oct. 5, 2006; accepted for publication Oct. 6, 2006; published online Apr. 9, 2007.

1 Introduction

Spectrometers or wavelength-division multiplexing (WDM) devices are utilized in various applications, such as biochemical analysis, remote sensing, fiber communications, and biosensing. A conventional spectrometer, which is based on a planar grating, has a sophisticated arrangement of optical components. A collimation lens (or mirror) and a focusing lens (or mirror) are typically required for such a planar grating system. Various microelectromechanical system (MEMS) fabrication techniques have been proposed to reduce the size of the spectrometer. Most of these MEMS-based spectrometers involve the use of moving parts to disperse wavelengths. Such parts are always associated with problems of mechanical instability.

This work employs a concave micrograting to reduce the size of a spectrometer without the problems of using moving components. The fabricated micrograting has a circular cylindrical surface profile. The grating structure is embedded inside a mirror-planar waveguide as presented in Fig. 1(b). The design, simulation, fabrication, and measurement of such a micrograting are described here.

2 Design and Simulation

The concave micrograting is embedded inside a mirror-planar waveguide, as shown in Fig. 1(b), to reduce dramatically the size of the spectrometer. The micrograting has a circular cylindrical surface profile. In the meridional plane (wavelength dispersion plane of the grating), the Rowland-circle configuration was adopted. It has the advantage of performing simultaneous wavelength dispersion and beam focusing, as shown in Fig. 1(a): beams of different wavelength are focused at different locations on the Rowland circle.[1–4] The grating is blazed to increase the diffraction efficiency of the specified diffraction order.[1–3] This chip spectrometer [Fig. 1(b)] covers wavelengths from 1475 to 1625 nm.

The determination of the grating line width (grating pitch) is based on the mask line width that can be achieved using standard mask fabrication. Consequently, our grating pitch is set to 3 μm, which can be easily fabricated using standard commercial mask fabrication technology. This 3-μm grating pitch was the starting point in the design, and the rest of the parameters were determined from a series of calculations and analyses of aberrations, spectral resolution, and the device's physical constrains.

An optical fiber is applied to guide the light into the chip spectrometer at point A in Fig. 1. The input optical fiber has a core size of 10 μm. The optical fiber has a core with a refractive index of 1.471 and a cladding with a refractive index of 1.460. These values correspond to a numerical aperture (NA) of 0.21, which produces a source angular divergence of 24.2 deg.[5] The source divergence must fulfill the following condition of total coherence to approach diffraction-limited performance:

$$\Delta\theta \leq \frac{2.44\lambda}{\Delta\sigma}, \quad (1)$$

where $\Delta\sigma$ and $\Delta\theta$ are the source size and the coherent angular divergence, respectively. With a source size of 10 μm, the condition in Eq. (1) yields an angular divergence of 21.7 deg. However, a wider angular divergence produces a larger aberration (with a circular cylindrical sur-

0091-3286/2007/$25.00 © 2007 SPIE

Downloaded From: http://opticalengineering.spiedigitallibrary.org/ on 04/26/2014 Terms of Use: http://spiedl.org/terms

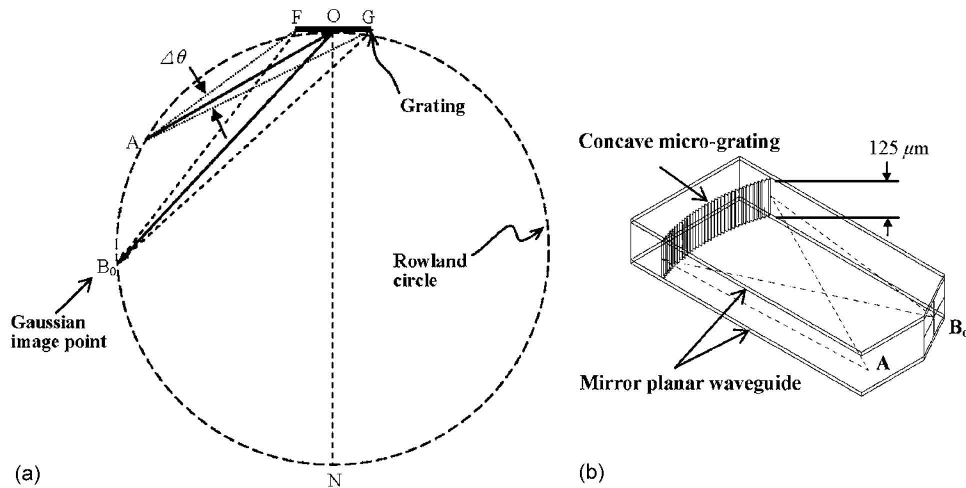

Fig. 1 (a) Rowland-circle configuration of the circular cylindrical micrograting. Point *A* is the input fiber source. Point B_0 is the Gaussian image point of the focused beam with a certain diffraction order. The arc *FG* represents the concave micrograting. The line *ON* is the normal to the grating. (b) Schematic of a concave micrograting embedded inside a mirror-planar waveguide.

face profile), which degrades the spectral resolution. Therefore, the angular divergence is limited to a certain value to ensure satisfactory spectral resolution.

2.1 *Resolution Properties*

The calculation of the aberration of the presented concave micrograting is based on optical-path-function analysis. Figure 2 presents the geometry used in the analysis of a reflective grating. For a diffraction grating, the optical path function of a ray that originates from point *A*, arrives at point $P(\xi, w, l)$ on the grating, and diffracts to point *B* on the detector is as follows[2,3]:

$$F = \overline{AP} + \overline{PB} + \frac{m\lambda}{d}w, \tag{2}$$

where *d* is the grating line constant, *m* is the order of diffraction, λ is the wavelength of the beam that is diffracted, and *w* is the *y* position of point *P* in the dispersion plane. The goal is to analyze the relationship between the parameters of a Rowland-circle mounting and the aberration. The specified grating has a surface profile described by the following surface function:

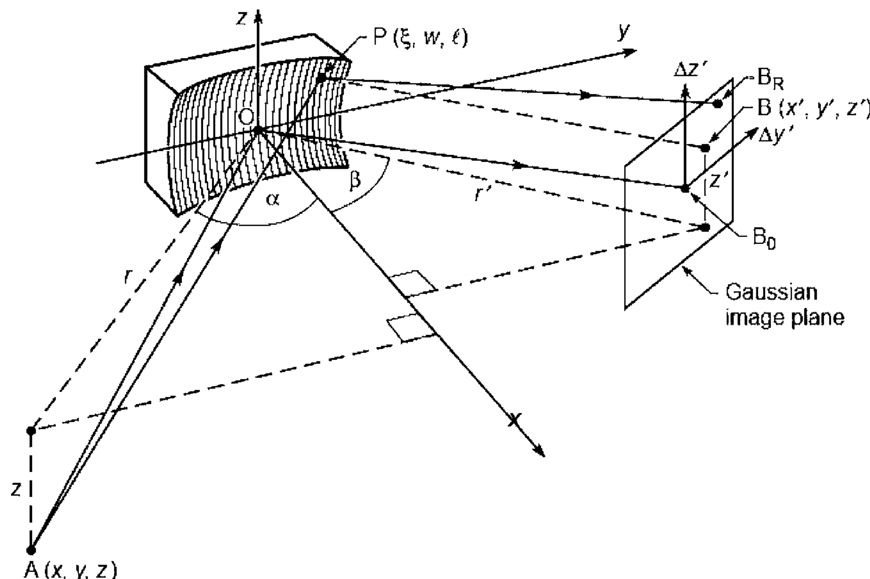

Fig. 2 Geometry of a concave reflective grating used in the aberration calculation. Point *A* is the source, and point B_0 is the Gaussian image point.

Downloaded From: http://opticalengineering.spiedigitallibrary.org/ on 04/26/2014 Terms of Use: http://spiedl.org/terms

Table 1 Factors contributing to the total spectral resolution.

Spectral width	Factor	Value (nm)
$\Delta\lambda_B$	Passband of the input wavelength	0.2
$\Delta\lambda_{S1}$	Entrance slit	0.2
$\Delta\lambda_{S2}$	Exit slit	0.2
$\Delta\lambda_{DL}$	Diffraction limit	0.2
$\Delta\lambda_A$	Aberration	0.8
$\Delta\lambda_{OSA}$	OSA resolution	0.1
$\Delta\lambda_{FE}$	Fabrication errors and other causes	0.0 (assumption)
$\Delta\lambda_{Total}$=	Total spectral resolution $=[(\Delta\lambda_B)^2+(\Delta\lambda_{S1})^2+(\Delta\lambda_{S2})^2+(\Delta\lambda_{DL})^2+(\Delta\lambda_A)^2+(\Delta\lambda_{OSA})^2]^{1/2}$ (Gaussian sum)	0.9

$$\xi=\sum_{i=0}^{\infty}\sum_{j=0}^{\infty}a_{ij}w^i l^j. \tag{3}$$

Based on Eq. (3), the optical path function F is expressed as follows[4]:

$$F=\sum_{ijk}F_{ijk}w^i l^j, \tag{4}$$

$$F_{ijk}=z^k C_{ijk}(\alpha,r)+z'^k C_{ijk}(\beta,r')+\frac{m\lambda}{d}w\,\delta_{(i-1)jk}. \tag{5}$$

In this case, a specific set of a_{ij} of the circular cylindrical surface is applied in Eq. (3).[4] In the dispersion plane of a Rowland-circle configuration [Fig. 1(a)], three major contributions to the total spectral resolution are considered.[2,3] They are contributions from the following:

1. Spectral width caused by the width of entrance slit (width S_1):

$$\Delta\lambda_{S1}=\frac{S_1 d\cos\alpha}{mr} \tag{6}$$

2. Spectral width caused by the width of exit slit (width S_2):

$$\Delta\lambda_{S2}=\frac{S_2 d\cos\beta}{mr'} \tag{7}$$

3. Spectral width due to the aberrations (of perfectly made grating):

$$\Delta\lambda_A=\frac{\Delta y' d\cos\beta}{mr'}=\frac{d}{m}\left(\frac{\partial F}{\partial w}\right) \tag{8}$$

4. Spectral width due to the diffraction limit:

Table 2 Parameters of the concave micrograting in the Rowland-circle configuration.

Parameter	Value
Operational wavelength range	1475 to 1625 nm
λ_c=central wavelength	1550 nm
α=incident angle	60 deg
β=exit angle	37.5 to 49.4 deg
m=diffraction order	3
d=grating constant (grating pitch)	3 μm
N=total line number	2584
R=horizontal (meridional) curvature of the grating surface profile	44.404 mm
ρ=vertical (sagittal) curvature of grating surface profile	∞
Horizontal width of grating (arc length FG in Fig. 1)	7.75 mm
Grating vertical height	125 μm
$\Delta\theta$=divergence angle of input source (□FAG in Fig. 1)	10 deg
S_1=core diameter of the input fiber (equivalent to the entrance-slit width of a conventional spectrometer)	10 μm
S_2=core diameter of the output fiber (equivalent to the exit-slit width of a conventional spectrometer)	10 μm

$$\Delta\lambda_{DL}=\frac{\lambda}{mN}. \tag{9}$$

In the calculation of the spectral width due to the aberration, the following major aberration terms are included: C_{040}, C_{100}, C_{120}, C_{140}, C_{200}, C_{220}, C_{240}, C_{300}, C_{400}, C_{420}, C_{500}, and C_{600}.[2,3] According to this calculation, the spectral width due to the aberration from Eq. (8) is 0.8 nm. The overall spectral resolution is the Gaussian sum of Eq. (6) to Eq. (9). Table 1 lists the result of the total spectral resolution.

The width of the entrance slit is the diameter of the core of the optical fiber, which is 10 μm. The performance in spectral resolution was measured using an optical fiber, which connects to an optical spectrum analyzer (OSA), in the image plane to acquire the spectral signals. A reasonable design depends on consideration of the choice of the rest of the parameters, such as the diffraction order m, the incident angle α, the exit angle β, the radius R of the Rowland circle, and the angular divergence $\Delta\theta$. Trade-offs must be made between the spectral resolution and the physical constrains of the device. To optimize the design, a design flow was developed to determine these parameters by taking account of the physical constraints and the required

Downloaded From: http://opticalengineering.spiedigitallibrary.org/ on 04/26/2014 Terms of Use: http://spiedl.org/terms

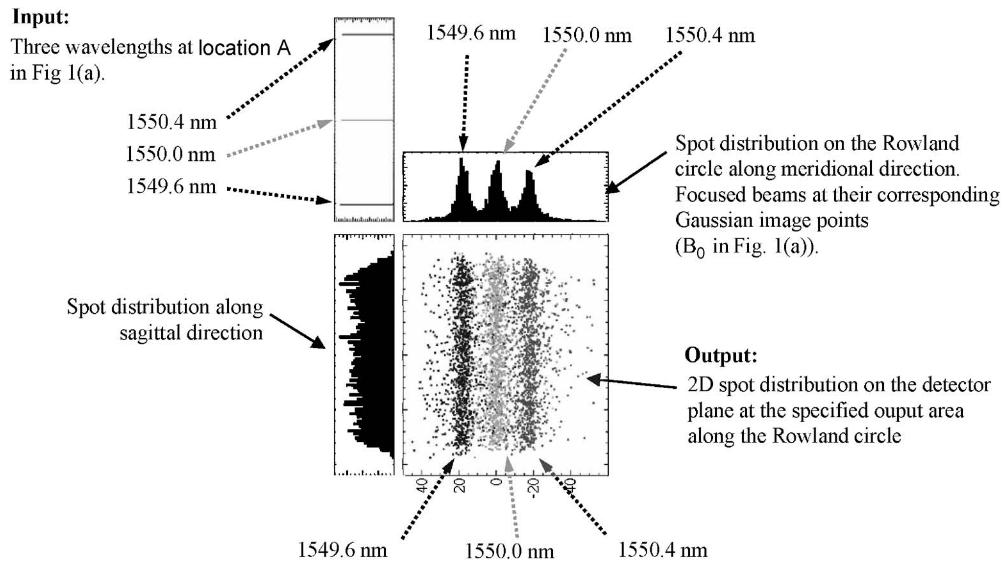

Fig. 3 Result of the ray tracing using the SHADOW program.

spectral resolution, such as the size of the chip, the location of the input fiber, the location of the output detecting area, the grating pitch, and the required spectral resolution. The specifications in Table 2 of the micrograting using a Rowland-circle configuration were obtained by this approach.

2.2 *Ray Tracing*

A ray-tracing simulation was performed using the SHADOW program to verify the results of the aberration calculations.[6] Figure 3 shows the spot diagram of the results obtained using the values of the parameters in Table 2. The input source [at location A in Fig. 1(a)] consists of three wavelengths: 1549.6, 1550.0, and 1550.4 nm (separated by 0.4 nm). A detecting plane (the Gaussian image plane in Fig. 2) in the SHADOW simulator is located at the output location of the focused beam on the Rowland circle [point B_0 in Figs. 1(a) and 2]. As presented in Fig. 3, the three input wavelengths are well resolved spatially on the Rowland circle. The input source has a size of 10 μm. The spot distribution in Fig. 3 reveals that each output focused beam has a width of 10 μm (which is the width of the distribution of the spots on the Rowland circle in the meridional direction in Fig. 3 at each wavelength) and the separation between adjacent focused beams is 20 μm. These results are consistent with those obtained from the calculation of the aberration based on the optical-path-function approach just described.

2.3 *Diffraction Efficiency*

Due to physical limitations, the third-order diffraction was used in the presented device, instead of the first-order diffraction, which has the largest diffraction efficiency for a laminar grating. Typical diffraction efficiencies of higher diffraction orders are very low for laminar gratings.[1–3] The use of a blazed grating overcomes this difficulty.[1,3] The diffraction efficiency of the specified diffraction order is greatly increased by choosing an appropriate pair of blaze angles (left blaze angle and right blaze angle).

The benefit of using lithography to fabricate blazed gratings is evident: it offers the freedom to select the blaze angles. In the fabrication procedure implemented herein, an Au coating is deposited on the grating surface to increase the reflectivity for this optical wavelength range. Also, in reality, the grating surface has a certain roughness. An 80-nm-thick Au coating with a root-mean-square (rms) surface roughness of 50 nm is used in the calculation of diffraction efficiency to simulate the actual fabrication conditions. Under these conditions, scalar diffraction theory does not apply. Instead, vector electromagnetic theory for gratings with boundary conditions must be adopted for the calculation.[7,8] An optimization process increases the third-order diffraction efficiency to a maximum of 60% to 70% [Fig. 4(b)] over the entire spectral range by using a 53-deg left blaze angle and an 81-deg right blaze angle [Fig. 4(a)], which are the pair of blaze angles used in the fabrication of the blazed grating herein.

3 Fabrication

The vertical height of the grating is designed to match the external diameter of the cladding of the optical fiber, which is 125 μm, as displayed in Fig. 1(b). This work utilizes deep x-ray lithography (DXL) to fabricate the cylindrical concave micrograting, since it is capable of producing a high aspect ratio, high spatial resolution, and excellent lithographic quality for optical applications.

A traditional x-ray photoresist (PMMA) has very low lithographic sensitivity and contrast. Therefore, a thin mask membrane and a thick mask absorber must be employed to block the x-ray irradiation in mask pattern transferring. Such a mask structure is very fragile and difficult to fabricate. Previous experimental results have demonstrated that SU-8 photoresist can provide very high lithographic contrast and sensitivity.[9] Hence, its corresponding x-ray mask absorber becomes thinner and the mask membrane thicker. Consequently, the complexity of the mask fabrication is substantially reduced. An x-ray mask with a thick Si membrane (5 μm) and a thin Au absorber (4 μm) was applied

Downloaded From: http://opticalengineering.spiedigitallibrary.org/ on 04/26/2014 Terms of Use: http://spiedl.org/terms

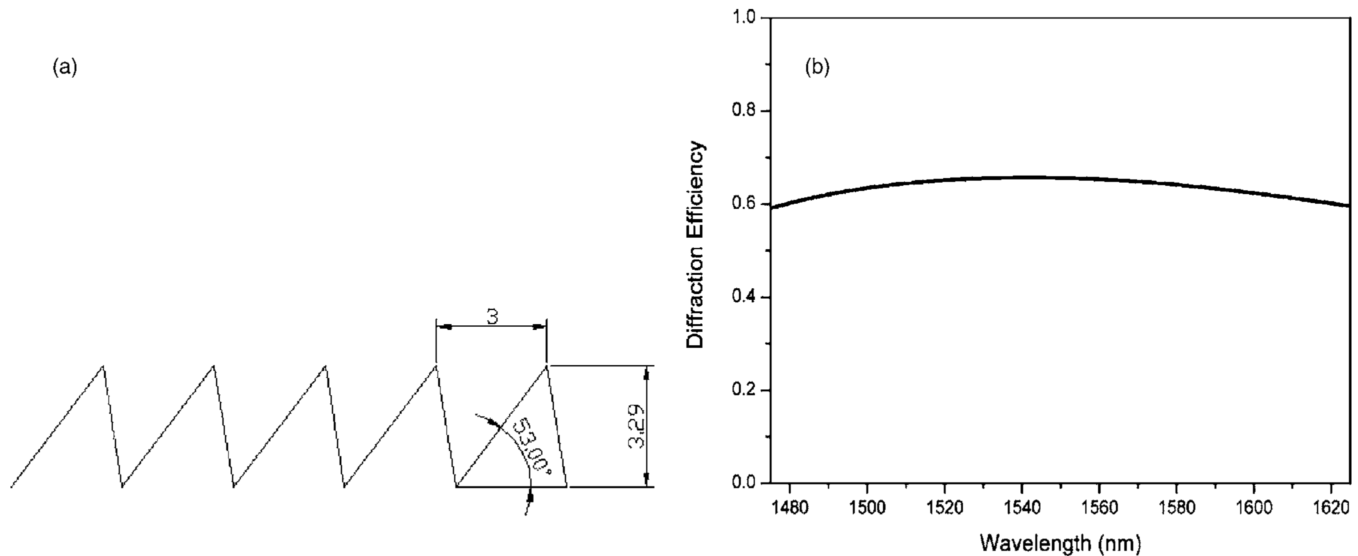

Fig. 4 (a) Blazed grating with 3-μm grating pitch, 53-deg left blaze angle, and 81-deg right blaze angle. (b) The diffraction efficiency of the third order versus wavelength (from 1475 to 1625 nm). Using the blaze setting in (a), the third-order efficiency reaches about 65%.

herein to pattern a cylindrical grating. A separate paper will discuss this novel x-ray mask technology used in the x-ray LIGA process.

Figure 5 displays scanning electron microscope (SEM) images of the concave micrograting fabricated using this DXL process. The 125-μm grating height and the 3-μm grating pitch were successfully achieved as presented in Fig. 5(a) and 5(b), respectively. The aspect ratio is 40. The developed DXL process also yields a perfect perpendicular sidewall with a vertical angle of better than 89.9 deg. Atomic force microscopy (AFM) was applied to a scan area of 1×1 μm and reveals a rms surface roughness of 5 nm. (The typical requirement for satisfactory optical performance is 50 nm.)

The rounding of the blaze angle displayed in Fig. 5(b) is caused by edge diffraction from the mask during the lithographic process in the making of an x-ray mask from an UV mask. The rounding effect can be considerably reduced by using an electron-beam writer to generate the mask pattern (a study of which effect will be undertaken in the future). After this grating was fabricated, an Au coating was deposited to a thickness of 80 nm on the grating surface to increase the reflectivity in this wavelength range. The efficiency calculation shows that the diffraction efficiency is reduced from 65% to 45% due to the rounding of the blaze.

A technology based on DXL was demonstrated to be able to produce grating patterns with very high precision for optical applications. A separate article will discuss in detail the fabrication process of this concave micrograting using DXL technology.

4 Resolution Measurements

The concave micrograting is embedded in a mirror-planar waveguide [Fig. 1(b)]. The waveguide comprises two parallel mirrors, which are Si wafers coated with Au (150 nm). This structure constitutes a spectrometer chip, as shown in Fig. 1(b).

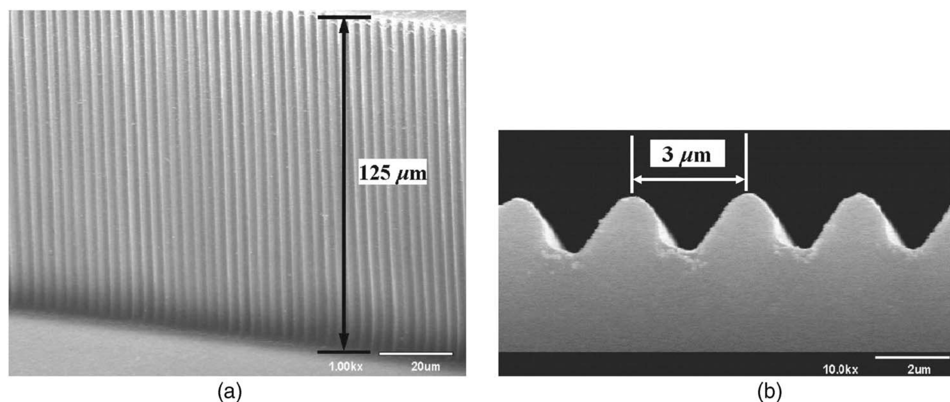

Fig. 5 SEM images of the SU-8 micrograting fabricated by the DXL process. (a) A height of 125 μm is achieved. (b) Top view of the grating. The rounding of the blaze was caused by the accuracy degradation in exposure during the pattern transfer from UV mask to x-ray mask.

Downloaded From: http://opticalengineering.spiedigitallibrary.org/ on 04/26/2014 Terms of Use: http://spiedl.org/terms

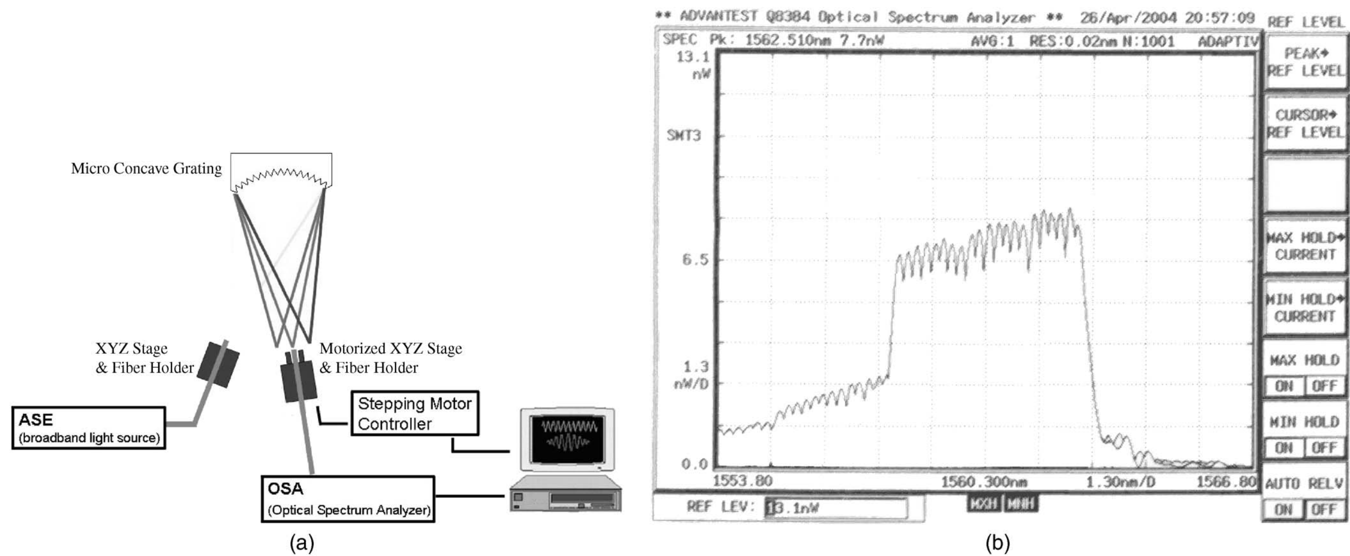

Fig. 6 (a) Schematic of the measurement setup. Here 21 separate wavelengths were fed into the fiber. The fiber at the output area was spatially scanned. (b) Acquired spectra with a scanned distance of 200 μm. A total of 21 peaks in the spectra are clearly resolved with a peak-to-peak spectral separation of 0.26 nm.

Figure 6(a) depicts the first performance measurement scheme. The input wavelengths are fed into the input fiber that is connected to this spectrometer chip. At the output location, an optical fiber with a core diameter of 10 μm is used to acquire the diffracted rays from the grating. The output fiber is connected to an OSA to analyze the spectral characteristics. In this performance test, 21 separate wavelengths were fed into the fiber. The front end of the fiber was spatially scanned across the focused region of the 21 wavelengths. Figure 6(b) presents the acquired data. The scanned distance is 200 μm. A total of 21 peaks in the spectrum are clearly resolved with a peak-to-peak spectral separation of 0.26 nm.

A second performance measurement of the spectral resolution of the concave micrograting was made using this chip-based spectrometer. Figure 7(a) presents the measurement scheme. Two DWDM channels of different wavelengths are coupled and fed into the input fiber. The measurements are made at two locations. Each location corresponds to the focal point of the specified input wavelength. The OSA displays two spectra for each input wavelength.

Rayleigh's criterion yields a measured FWHM spectral width (spectral resolution) of 1.1 nm. This measurement is compared with the calculated value using the contributing factors that are presented in Table 1. The total spectral

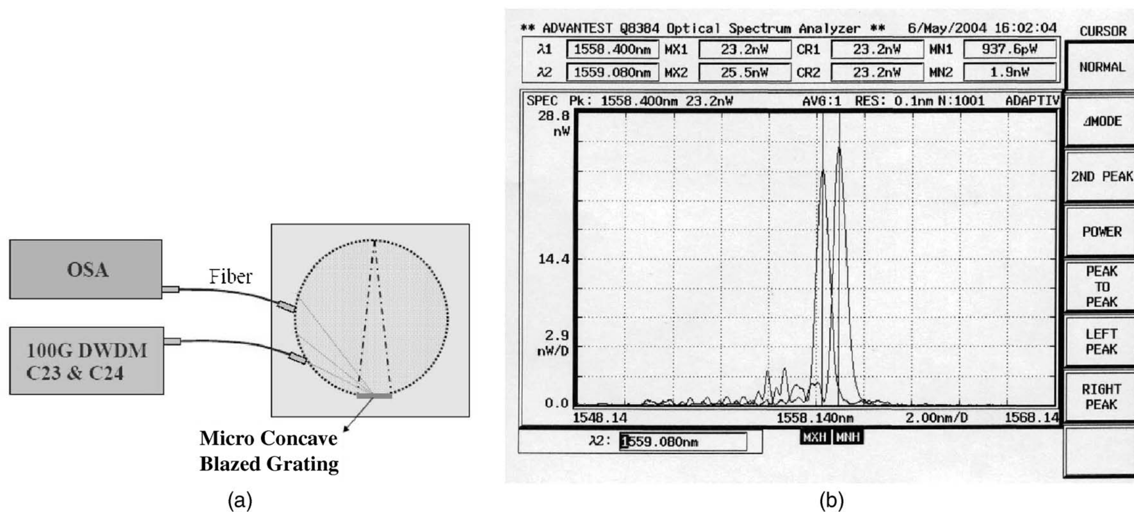

Fig. 7 (a) Schematic of the second measurement scheme. Two DWDM channels of different wavelengths are coupled and fed into the input fiber. The measurements were made at two locations corresponding to the focal point of the specified input wavelength. (b) Acquired spectra. The data yields a FWHM spectral width (spectral resolution) of 1.1 nm using Rayleigh's criterion.

Downloaded From: http://opticalengineering.spiedigitallibrary.org/ on 04/26/2014 Terms of Use: http://spiedl.org/terms

width $\Delta\lambda_{Total}$ is the Gaussian sum of each individual contribution as presented in Table 1. The spectral width associated with the fabrication error ($\Delta\lambda_{FE}$) in Table 1 is assumed to be zero. The Gaussian sum of these factors yields a total spectral resolution $\Delta\lambda_{Total}$ of 0.9 nm. The result agrees very closely with the measured value of 1.1 nm.

5 Conclusions

This investigation has demonstrated that the developed spectrometer-chip scheme based on a micrograting that is embedded inside a planar waveguide works. DXL fabrication technology is very powerful in fabricating this concave micrograting. An aspect ratio of 40 in the grating structure is achieved. The confirmation of the results of the aberration calculation and the ray tracing by the measurements indicates that the chip-based spectrometer functions as designed. DXL based on the SU-8 photoresist can be further developed into an x-ray LIGA technique for mass-producing concave microgratings. Future advances in such fabrication approaches will produce low-cost polymer-based spectrometer chips with good spectral resolution.

Acknowledgments

The authors would like to thank the National Science Council of the Republic of China, Taiwan (contract No. NSC-94-2215-E-155-002) and the China Steel Corporation for financially supporting this research. Mao-Chang Liang, Chin-Chien Lui, and Chi-Kang Lo are thanked for making the calculations and conducting performance tests. The testing was performed at the Optical Fiber Testing Laboratory of the Department of Electro-Optical Engineering, Vanung University, Taiwan. The authors would also like to thank Prof. L. G. Sheu and Mr. C. M. Chen of Vanung University for valuable discussions and helping with the testing and measurements. The staff at NSRRC provided wonderful service during our experiments. We would like also to thank Mr. S. F. Cheng for cutting the Si wafer, and Dr. Ping-Chung Tseng at NSRRC for a valuable discussion on the SHADOW program.

References

1. M. C. Hutley, *Diffraction Gratings*, Academic, London (1982).
2. W. B. Peatman, *Gratings, Mirrors and Slits: Beamline Design for Soft X-Ray Synchrotron Radiation Sources*, Gordon and Breach Science, Singapore (1997).
3. A. C. Thompson and D. Vaudhn, Eds., *X-Ray Data Booklet*, 2nd ed., Center for X-ray Optics, Lawrence Berkeley Laboratory (2001).
4. M. Born and E. Wolf, *Principle of Optics*, 7th ed., Cambridge Univ. Press, Cambridge, UK (1999).
5. B. E. A. Saleh and M. C. Teich, *Fundamentals of Photonics*, 2nd ed., Wiley, New York (1991).
6. http://www.esrf.fr/computing/scientific/xop/shadowvui/
7. M. Neviere, P. Vincent, and D. Maystre, "X-ray efficiencies of gratings," *Appl. Opt.* **17**, 843–845 (1978).
8. R. Petit, *Electromagnetic Theory of Gratings*, Springer-Verlag, Berlin (1980).
9. B. Y. Shew, T. Hung, T. Y. Huang, K. P. Liu, and C. P. Chou, "High resolution x-ray micromachining using SU-8 resist," *J. Micromech. Microeng.* **13**(5), 708–713 (2003).

Cheng-Hao Ko received his PhD and master's degrees in physics from the State University of New York at Stony Brook in 1995 and 1990, respectively. He received his BS in physics from National Taiwan University, Taiwan, at 1985. His doctoral research was on x-ray microscopy combined with electron spectroscopy for chemical analysis (ESCA). In his doctoral research, he built the world's first multichannel scanning photoemission microscope (SPEM), which was located at Beamline X1A of the National Synchrotron Light Source (NSLS) at Brookhaven National Laboratory (BNL), USA. After his PhD, Dr. Ko joined the staff at the National Synchrotron Radiation Research Center (NSRRC), Taiwan, as an associate research scientist. He led a team to construct the first scanning photoemission microscope in Asia. Dr. Ko is currently a professor at Yuan Ze University, Taiwan. His current research interests include spectrum chip fabrication, CMOS photonic crystal devices, and MEMS/MOEMS-based biosensors.

Bor-Yuan Shew received his BS in mechanical engineering in 1989 from National Cheng-Kung University, Taiwan. He then finished his master's degree and PhD in material engineering at the same university at 1991 and 1996, respectively. He is now an associate research scientist and the leader of the device technology group at the National Synchrotron Radiation Research Center (NSRRC), Taiwan. His current research interests include nanofabrication, LIGA technology, MEMS/MOEMS, and biosensors.

Shih-Che Hsu: Biography and photograph not available.

Downloaded From: http://opticalengineering.spiedigitallibrary.org/ on 04/26/2014 Terms of Use: http://spiedl.org/terms